Interaction cross sections and matter radii of oxygen isotopes using the Glauber model

Suhel Ahmad, A. A. Usmani, Shakeb Ahmad, and Z. A. Khan*
Department of Physics, Aligarh Muslim University, Aligarh 202 002, India
(Received 13 December 2016; revised manuscript received 8 March 2017; published 1 May 2017)

Using the Coulomb modified correlation expansion for the Glauber model S matrix, we calculate the interaction cross sections of oxygen isotopes ($^{16-26}$O) on ^{12}C at 1.0 GeV/nucleon. The densities of $^{16-26}$O are obtained using (i) the Slater determinants consisting of the harmonic oscillator single-particle wave functions (SDHO) and (ii) the relativistic mean-field approach (RMF). Retaining up to the two-body density term in the correlation expansion, the calculations are performed employing the free as well as the in-medium nucleon-nucleon (NN) scattering amplitude. The in-medium NN amplitude considers the effects arising due to phase variation, higher momentum transfer components, and Pauli blocking. Our main focus in this work is to reveal how could one make the best use of SDHO densities with reference to the RMF one. The results demonstrate that the SDHO densities, along with the in-medium NN amplitude, are able to provide satisfactory explanation of the experimental data. It is found that, except for ^{23,24}O, the predicted SDHO matter rms radii of oxygen isotopes closely agree with those obtained using the RMF densities. However, for ^{23,24}O, our results require reasonably larger SDHO matter rms radii than the RMF values, thereby predicting thicker neutron skins in ^{23}O and ^{24}O as compared to RMF ones. In conclusion, the results of the present analysis establish the utility of SDHO densities in predicting fairly reliable estimates of the matter rms radii of neutron-rich nuclei.

DOI: 10.1103/PhysRevC.95.054601

I. INTRODUCTION

The rapid progress in the accelerator and detection techniques around the globe has made it possible to produce and study unstable nuclei away from the stability line. This development has added new dimensions in the fields of both nuclear physics and nuclear astrophysics. The unstable neutron-rich nuclei play an important role in the formation of ultra-neutron-rich and superheavy nuclei near the nascent neutron star. The formation of such nuclei is the result of the nuclear reactions and fusion phenomena in the cosmological objects. The study of the results of various observations, such as the nuclear reaction cross sections, elastic scattering differential cross sections, one-nucleon removal cross sections, and Coulomb breakup cross sections makes it possible to extract information about the detailed structure of these unstable nuclei, particularly the halo structure near the drip lines. Impetus to the field of unstable neutron-rich nuclei, however, came more into existence only after the results of Tanihata *et al.* [1], who discovered the neutron halo in ^{11}Li. Subsequently, the matter radii of neutron-rich nuclear isotopes have been quite effectively derived from the measurement of reaction cross sections [2]. A nuclear halo is manifested by a sudden increase in the reaction cross section and hence the matter radius of a nucleus compared to its neighboring isotopes. Such a structure has been considered as the one having one or two weakly bound valence neutrons, which allows the tunneling of the wave function into the classically forbidden region, thereby forming a low-density neutron halo around the core. This feature of extended neutron distribution has also been observed in ^{11}Be [3,4] and ^{19,22}C [5–8], and ^{31}Ne in the so-called island of inversion region [9].

Due to limited experimental information on the neutron drip line for $Z > 8$, the production of oxygen isotopes from $A = 16$ to 28 may be considered as the heaviest nuclei for which a neutron drip line has been well established. The interaction cross-section (σ_I) data for oxygen isotopes up to the drip-line nucleus ^{24}O are available at relatively high energies ($\sim$1.0 GeV/nucleon) [2]. These cross sections show a smooth increase with increasing neutron number from ^{16}O to ^{21}O and then a sudden increase up to ^{23}O. The sharp increase in σ_I for ^{23}O supports the idea of ^{23}O being a one-neutron halo and having large matter radius, although its relatively high one-neutron separation energy ($\sim$2.74 MeV) [2] favors it to have a nonhalo structure. To explore the anomaly in the interaction cross section of ^{23}O, Kanungo *et al.* [10] have revised the measurements of σ_I of ^{22,23}O-^{12}C at $\sim$900 MeV/nucleon. The new data show that σ_I for ^{23}O is smaller than that reported earlier. The value of σ_I for ^{23}O in the revised data is only $\sim$8–9% larger than that for ^{22}O, which may not be sufficient to classify ^{23}O as a one-neutron halo.

In a recent analysis [11], we have calculated the interaction cross sections of neon isotopes $^{17-32}$Ne on ^{12}C at 240 MeV/nucleon within the framework of Coulomb modified correlation expansion for the Glauber model (CMGM) S matrix. The results suggested that the use of the Slater determinant description of colliding nuclei, involving harmonic oscillator single-particle wave functions (hereafter referred to as SDHO densities), can be considered as a good starting point to predict the matter root-mean-square (rms) radii of stable as well as (exotic) neutron-rich nuclei.

Motivated by the successful application of CMGM to analyzing the differential cross section and reaction cross section of nucleon-nucleus and nucleus-nucleus collisions at intermediate energies, we, in this work, propose to undertake the analysis of the interaction cross sections of oxygen isotopes, $^{16-24}$O, on ^{12}C at $\sim$1.0 GeV/nucleon within the

*zakhan.amu@gmail.com

framework of CMGM. The calculations consider up to the two-body density term in the correlation expansion, which is expected to provide the dominant correction to the uncorrelated part. Keeping in view the effective use of SDHO densities in predicting the nuclear matter rms radii, particularly for the neutron-rich nuclei near the drip lines, the calculations involve SDHO densities for oxygen isotopes. To test the usefulness of SDHO densities, we also consider the relativistic mean field (RMF) densities, obtained in this work, in calculating the interaction cross sections of oxygen isotopes. Our aim in this work is to see how far the considered densities account for the available experimental data and what could be said about the use of SDHO densities in predicting the matter rms radii of oxygen isotopes.

A brief formulation of the problem is given in Sec. II. The numerical results are presented and discussed in Sec. III. The conclusions are presented in Sec. IV.

II. FORMULATION

According to the Glauber model, the scattering amplitude describing the elastic scattering of a projectile nucleus with ground-state wave function ψ_B on a target nucleus with ground-state wave function ψ_A may be written as [12,13]

$$F_{el}(\vec{q}) = \frac{iK}{2\pi}\int e^{i\vec{q}.\vec{b}}[1 - S_{el}(\vec{b})]d^2b, \tag{1}$$

$$S_{el}(\vec{b}) = \langle\psi_A\psi_B|\prod_{i=1}^{A}\prod_{j=1}^{B}[1 - \Gamma_{NN}(\vec{b} - \vec{s}_i + \vec{s}_j^{'})]|\psi_B\psi_A\rangle, \tag{2}$$

where $A(B)$ is the mass number of target(projectile) nucleus, $\vec{b}$ is the impact parameter vector perpendicular to the incident momentum $\vec{K}$, $\vec{s}_i(\vec{s}_j^{'})$ are the projections of the target(projectile) nucleon coordinates on the impact parameter plane, and $\Gamma_{NN}(\vec{b})$ is the nucleon-nucleon (NN) profile function, which is related to the NN scattering amplitude $f_{NN}(\vec{q})$ as follows:

$$\Gamma_{NN}(\vec{b}) = \frac{1}{2\pi ik}\int e^{-i\vec{q}.\vec{b}}f_{NN}(\vec{q})d^2q, \tag{3}$$

where k is the incident nucleon momentum corresponding to the projectile kinetic energy per nucleon and $\vec{q}$ is the momentum transfer.

To obtain the correlation expansion for the Glauber model S matrix, we follow Ahmad [14], according to which the S-matrix element S_{el} is rewritten as

$$S_{el}(\vec{b}) = \langle\psi_A\psi_B|\prod_{i=1}^{A}\prod_{j=1}^{B}[(1 - \Gamma_{00}) + \gamma_{ij}]|\psi_B\psi_A\rangle, \tag{4}$$

where

$$\gamma_{ij} = \Gamma_{00} - \Gamma_{NN}(\vec{b} - \vec{s}_i + \vec{s}_j^{'}) \tag{5}$$

and

$$\Gamma_{00} = \int \rho_A(\vec{r})\rho_B(\vec{r}^{'})\Gamma_{NN}(\vec{b} - \vec{s} - \vec{s}^{'})d\vec{r}d\vec{r}^{'}. \tag{6}$$

The quantities ρ_A and ρ_B in Eq. (6) are the (one-body) ground-state densities of the target and projectile, respectively.

Now, it is found that the double product in Eq. (4) gives the following expression for the S-matrix element S_{el}:

$$S_{el}(\vec{b}) = S_0(\vec{b}) + \sum_{l=2}^{AB} S_l(\vec{b}), \tag{7}$$

where

$$S_0(\vec{b}) = (1 - \Gamma_{00})^{AB} \tag{8}$$

and

$$S_l(\vec{b}) = \langle\psi_A\psi_B|\frac{1}{l!}(1 - \Gamma_{00})^{AB-l}{\sum_{i_1,j_1}}'{\sum_{i_2,j_2}}'\cdots$$
$$\times {\sum_{i_l,j_l}}'\gamma_{i_1,j_1}\gamma_{i_2,j_2}\ldots\gamma_{i_l,j_l}|\psi_B\psi_A\rangle. \tag{9}$$

The primes on the summation signs indicate the restriction that two pairs of indices cannot be equal at the same time (for example, if $i_1 = i_2$ then $j_1 \neq j_2$ and vice versa). Moreover, the sum in Eq. (7) starts from $l = 2$, as the $l = 1$ term does not contribute to the elastic scattering.

Further, it is found that the substitution of expansion (7) in Eq. (1) leads to the required correlation expansion for the elastic scattering amplitude

$$F_{el}(\vec{q}) = F_0(\vec{q}) + \sum_{l=2}^{AB} F_l(\vec{q}), \tag{10}$$

where

$$F_0(\vec{q}) = \frac{iK}{2\pi}\int e^{i\vec{q}.\vec{b}}[1 - S_0(\vec{b})]d^2b \tag{11}$$

and

$$F_l(\vec{q}) = -\frac{iK}{2\pi}\langle\psi_A\psi_B|S_l|\psi_B\psi_A\rangle. \tag{12}$$

The term F_0 in Eq. (10) is the uncorrelated part of the scattering amplitude, involving all orders of scattering and depends upon the one-body densities of the colliding nuclei through Γ_{00} [Eq. (6)]. The other terms F_l ($l \geqslant 2$) involve the lth-body density of both the target and projectile nuclei and may be regarded as providing corrections to the uncorrelated part. As mentioned in Sec. I, we consider only up to $F_2(S_2)$ term in Eq. (10) [Eq. (7)], which is expected to provide a leading correction to the uncorrelated part; the detailed evaluation of $F_2(S_2)$ follows a similar approach as discussed in Ref. [14].

The Coulomb scattering has been incorporated in the same way as suggested in Ref. [15]. Further, the deviation in the straight-line trajectory of the Glauber model because of the Coulomb field can be incorporated [16] by replacing b in $S_{el}(\vec{b})$ [Eq. (4)] by $b^{'}$, which is the distance of the closest approach in Rutherford orbits and is given by

$$kb^{'} = \eta + (\eta^2 + k^2b^2)^{1/2}, \tag{13}$$

where $\eta = Z_AZ_Be^2/\hbar v$ is the Sommerfeld parameter with $Z_A(Z_B)$ as the target (projectile) atomic number and v is the projectile-target relative velocity.

With these considerations, the elastic differential cross section is calculated using the expression

$$\frac{d\sigma}{d\Omega} = |F_{el}(\vec{q})|^2. \tag{14}$$

In connection with the interaction cross section (σ_I), it may noted that, at relativistic energies, the inelastic cross section (σ_{inela}) is smaller than the typical errors of σ_I and, therefore, σ_I can be assumed to be nearly equal to the reaction cross section (σ_R) [17]. Hence, the Glauber model S matrix [Eq. (7)] can be used to calculate both σ_I and σ_R as follows:

$$\sigma_{I(R)} = \int d^2b[1 - |S_{el}(\vec{b})|^2]. \tag{15}$$

Finally, it should be noted that the above formulation can also be used for hadron-nucleus collision [18]. For this, we need to drop all the quantities related to the projectile and set $\text{B} = Z_B = 1$.

III. RESULTS AND DISCUSSION

Following the approach outlined in Sec. II, we have calculated the interaction cross sections (σ_I) of $^{16\text{–}26}$O on ^{12}C at 1.0 GeV/nucleon. The inputs required in the calculation are (i) the NN scattering amplitude, (ii) the proton and neutron density distributions of colliding nuclei, and (iii) the oscillator parameters.

In the first phase of our calculations, the NN scattering amplitude is parametrized in the form [19]

$$f_{NN}(\vec{q}) = \frac{k\sigma_{NN}}{4\pi}(i + \rho_{NN})e^{-\beta_{NN}q^2/2}, \tag{16}$$

where σ_{NN} is the NN total cross section, ρ_{NN} is the ratio of the real to the imaginary parts of the forward NN amplitude, and β_{NN} is the slope parameter. The values of σ_{NN}, ρ_{NN}, and β_{NN} at energy under consideration are taken from Ref. [20]. Here it should be noted that the above-mentioned NN amplitude, with its parameter values in Ref. [20], describes the free NN scattering.

The proton and neutron density distributions of $^{16\text{–}26}$O isotopes are obtained using (i) the Slater determinants constructed from the harmonic oscillator single-particle wave functions (SDHO) and (ii) the relativistic mean field (RMF) approach. For SDHO densities, we follow similar approach to that outlined in Refs. [11,21]. The expressions for the SDHO proton and neutron density distributions of oxygen isotopes ($^{16\text{–}26}$O) are given in the appendix. To obtain the RMF proton and neutron density distributions for oxygen isotopes ($^{16\text{–}26}$O), we have performed calculations in an axially symmetric deformed basis with reflection symmetry. The force parameter $NL3^*$ has been used for the Lagrangian [22]. Pairing correlations have been treated within the BCS scheme with constant pairing gap [23]. The RMF densities of $^{16\text{–}26}$O, obtained in this way, are depicted in Figs. 1 and 2, and the corresponding root-mean-square (rms) radii for proton, neutron, and matter distributions are given in Table I. For the target nucleus ^{12}C, we use density distributions for the protons and neutrons, which are obtained by using the RMF approach [9].

The oscillator parameters (α^2) for SDHO proton and neutron density distributions are fixed from the corresponding

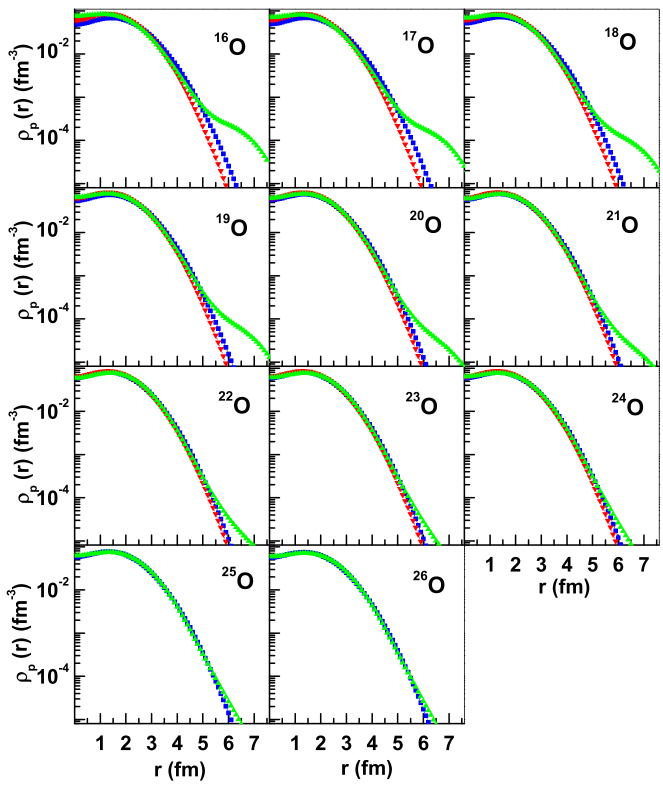

FIG. 1. Point-proton SDHO and RMF density distributions in $^{16\text{–}26}$O isotopes. Squares (inverted triangles) and triangles show, respectively, SDHO and RMF densities. The calculations of SDHO densities, shown by squares and inverted triangles, correspond to the values of oscillator parameters for proton distributions as given in Tables II and III, respectively.

relativistic mean field rms radii (Table I) for nuclei under consideration. The values of α^2 obtained in this way are given in Table II, and the SDHO proton and neutron distributions are presented in Figs. 1 and 2.

The results of the calculation for σ_I (with two-body density term) of $^{16\text{–}26}$O on ^{12}C at 1.0 GeV/nucleon using SDHO and RMF densities are presented in Fig. 3. It is found that both the SDHO and RMF densities provide similar accounts of the interaction cross sections. Further, it is to be noted that although the theoretical predictions show the increasing trend as observed in the experimental data [2], we observe large discrepancies between theory and experiment in almost all the cases. From the point of view of density, it is seen that although the densities under consideration (Figs. 1 and 2) are quite different, this difference is not significantly reflected in the σ_I results (Fig. 3). This shows that SDHO and RMF densities of $^{16\text{–}26}$O, with similar rms radii of proton and neutron distributions, may be considered on equal footing as far as the calculations of σ_I are concerned.

To look into the possible causes of source of discrepancy between theory and experiment, we now proceed to calculate the interaction cross sections of $^{16\text{–}24}$O on ^{12}C at 1.0 GeV/nucleon using the SDHO densities in which the oscillator parameters are varied up to the extent of getting better description of the data. In fact, the purpose of such calculations is to assess

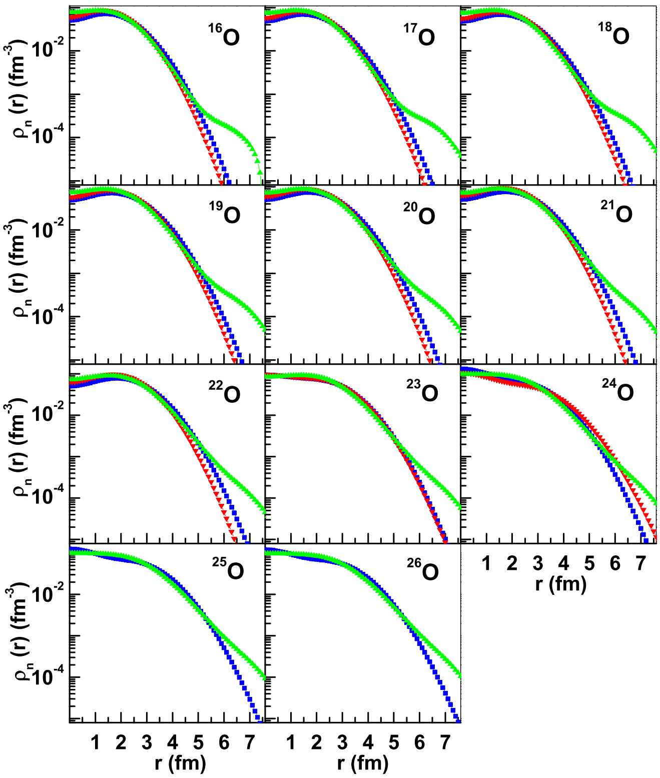

FIG. 2. Point-neutron SDHO and RMF density distributions in $^{16\text{–}26}$O isotopes. Squares (inverted triangles) and triangles show, respectively, SDHO and RMF densities. The calculations of SDHO densities, shown by squares and inverted triangles, correspond to the values of oscillator parameters for neutron distributions as given in Tables II and III, respectively.

how far a reasonable variation in the RMF matter rms radii of oxygen isotopes helps in accounting for the experimental data. To achieve this, the value of α^2 for proton distribution (α_p^2) in ^{16}O has been fixed from the interaction cross section of ^{16}O on ^{12}C at 1.0 GeV/nucleon, and it is the corresponding rms radius which has been assumed to be the same for all other oxygen isotopes. Thus the present calculations involve searching α^2 for neutron distribution (α_n^2) only for the isotopes $^{17\text{–}24}$O. The results of such calculations are shown in Fig. 4. The values of α_p^2 and α_n^2 obtained in this way, and the corresponding matter rms radii of oxygen isotopes are presented in Table III. We find that such an exercise though provides good account of the interaction cross-section data, the matter rms radii of $^{16\text{–}24}$O are found to be quite different from those obtained using RMF densities (Fig. 5). A similar situation has also been observed by Abu-Ibrahim *et al.* [24] in their calculations involving SDHO densities. To examine the extracted matter rms radii of oxygen isotopes (Table III) in other situations, we consider the analysis of the available experimental data on (i) p-^{16}O elastic differential cross sections at 200, 300, 600, and 1000 MeV and (ii) p-^{16}O reaction cross sections in the energy range 40–1000 MeV. The values of the parameters of the NN amplitude [Eq. (16)] at energies under consideration are taken from Ref. [20]. The results of these calculations are presented in Figs. 6 and 7. Here, we find that the extracted matter rms radius of ^{16}O helps to push theory closer to the experiment, but the results are not as satisfactory as the one observed in the case of ^{16}O-^{12}C interaction cross section (Fig. 4). As a result, the present calculations lead to inconclusive findings simply due to the fact that since the RMF densities work well for nonhalo nuclei [9], the significant deviation from the RMF matter rms radii may not be justified. Moreover, our major concern is the rms radius of ^{16}O nucleus which makes sense provided it is closer to the electron scattering value [28]. Unfortunately, the present calculation with SDHO density predicts smaller rms radius of ^{16}O (2.55 fm; Table III) as compared to those obtained using electron scattering experiments (2.73 fm; Ref. [28]) and RMF densities (2.72 fm; Table I). This suggests that instead of reproducing the interaction cross-section data at the cost of matter rms radii, one should explore the other possibilities to understand the source of discrepancy between theory and experiment.

Before proceeding further, it is important to reiterate that while performing the aforesaid calculations, we have used the experimental values of the NN total cross section (σ_{NN}) [20],

TABLE I. The calculated (RMF) proton (r_p), neutron (r_n), and matter (r_m) radii of oxygen isotopes.

Nucleus	r_p (fm)	r_n (fm)	r_m (fm)
^{16}O	2.75	2.70	2.72
^{17}O	2.74	2.84	2.79
^{18}O	2.71	2.93	2.83
^{19}O	2.67	2.97	2.85
^{20}O	2.64	3.01	2.87
^{21}O	2.63	3.04	2.89
^{22}O	2.62	3.00	2.92
^{23}O	2.62	3.16	2.99
^{24}O	2.63	3.25	3.05
^{25}O	2.65	3.33	3.13
^{26}O	2.68	3.39	3.19

TABLE II. The calculated oscillator parameters, α_p^2 and α_n^2, that, when used in SDHO densities, predict the rms radii, r_p and r_n (Table I), as obtained from the RMF proton and neutron density distributions, respectively.

Nucleus	α_p^2 (fm^{-2})	α_n^2 (fm^{-2})
^{16}O	0.286	0.295
^{17}O	0.288	0.286
^{18}O	0.296	0.281
^{19}O	0.305	0.284
^{20}O	0.312	0.286
^{21}O	0.316	0.287
^{22}O	0.318	0.286
^{23}O	0.318	0.277
^{24}O	0.317	0.267
^{25}O	0.312	0.258
^{26}O	0.305	0.251

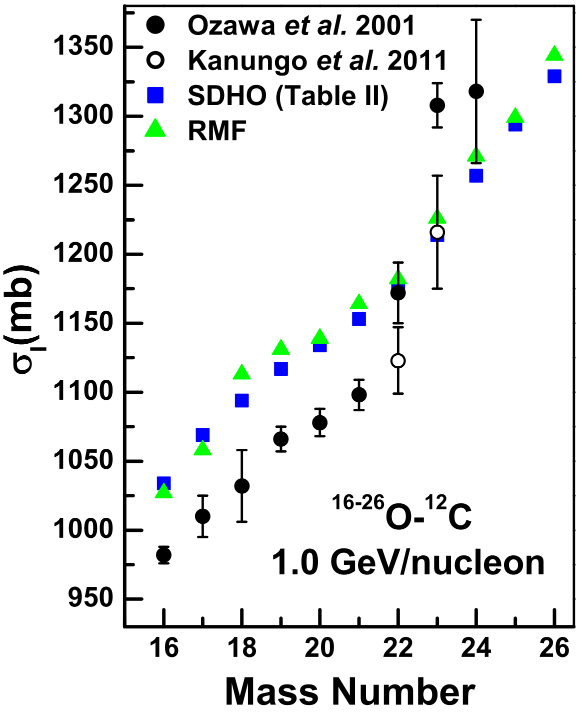

FIG. 3. Interaction cross sections of $^{16–26}$O isotopes on a ^{12}C target at 1.0 GeV/nucleon using SDHO (squares) and RMF (triangles) densities. The calculations using SDHO densities involve the values of oscillator parameters for proton and neutron distributions as given in Table II. The experimental data (dots and open circles) are taken from Ozawa *et al.* [2] and Kanungo *et al.* [10].

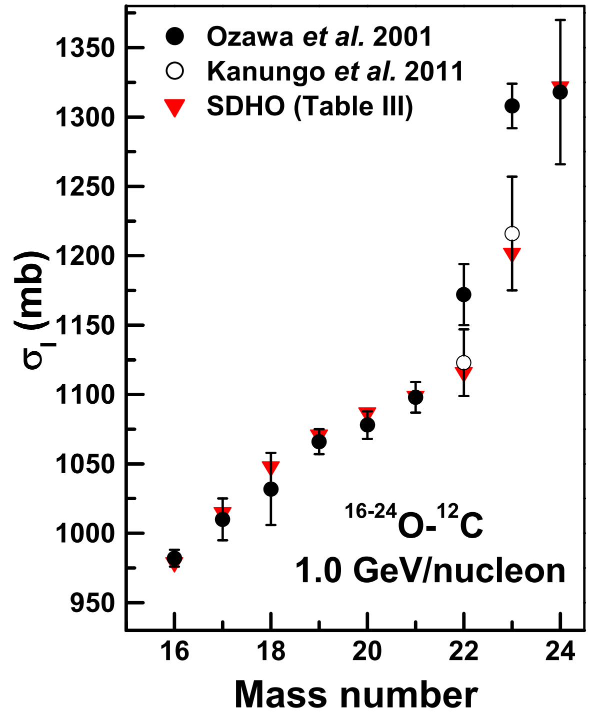

FIG. 4. Interaction cross sections of $^{16–24}$O isotopes on a ^{12}C target at 1.0 GeV/nucleon using SDHO (inverted triangles) densities. The calculations using SDHO densities involve the values of oscillator parameters for proton and neutron distributions as given in Table III. The experimental data (dots and open circles) are taken from Ozawa *et al.* [2] and Kanungo *et al.* [10].

which describes the free NN scattering. However, the earlier studies [29,30] demonstrated that in-medium NN total cross section is strongly modified by the Pauli blocking. Moreover, our results [31] have shown that it is not only the NN total cross section but also the other parameters of the NN amplitude (ρ_{NN} and β_{NN}) which get modified in the nuclear medium. Also, the consideration of phase variation [31] and higher momentum-transfer components [31] of the NN amplitude seems to be important in any realistic study of the nuclear cross-section data. Thus, keeping in view of the fact that the use of (free) NN amplitude along with SDHO densities demands large deviations in the so-called realistic (RMF) matter rms radii, we therefore propose to reanalyze the $^{16–24}$O interaction cross sections on ^{12}C at 1.0 GeV/nucleon using the SDHO densities corresponding to RMF matter rms radii, involving the phase variation, higher momentum transfer components, and Pauli blocking of the NN amplitude. Our aim is to see how far the efforts of using realistic form of the NN amplitude helps in accounting for the experimental data and what could be said about the use of SDHO densities in predicting the matter rms radii of oxygen isotopes.

In order to have physically meaningful results, we need to have in-medium parameters of the NN amplitude in the presence of its phase variation, higher momentum transfer components, and Pauli blocking at the energy under consideration, so that the calculations of the interaction cross sections become parameter free. For this purpose, we consider the analysis of p-^{16}O elastic scattering differential cross section at 1.0 GeV involving the SDHO densities with the same matter rms radius as obtained using the RMF densities (Table I). The calculations include systematic study of the effects arising due to phase variation, higher momentum transfer components, and Pauli blocking of the NN amplitude. The details of such calculations are described as below.

TABLE III. The calculated oscillator parameters, α_p^2 and α_n^2, that, when used in SDHO densities, provide good account of the interaction cross sections of $^{16–24}$O on ^{12}C at 1.0 GeV/nucleon. The last column gives the matter rms radii of $^{16–24}$O as predicted in these calculations.

Nucleus	α_p^2 (fm^{-2})	α_n^2 (fm^{-2})	r_m (fm)
^{16}O	0.332	0.332	2.55
^{17}O	0.332	0.319	2.62
^{18}O	0.333	0.311	2.69
^{19}O	0.334	0.313	2.72
^{20}O	0.334	0.321	2.73
^{21}O	0.335	0.329	2.74
^{22}O	0.335	0.330	2.76
^{23}O	0.336	0.281	2.95
^{24}O	0.336	0.231	3.21

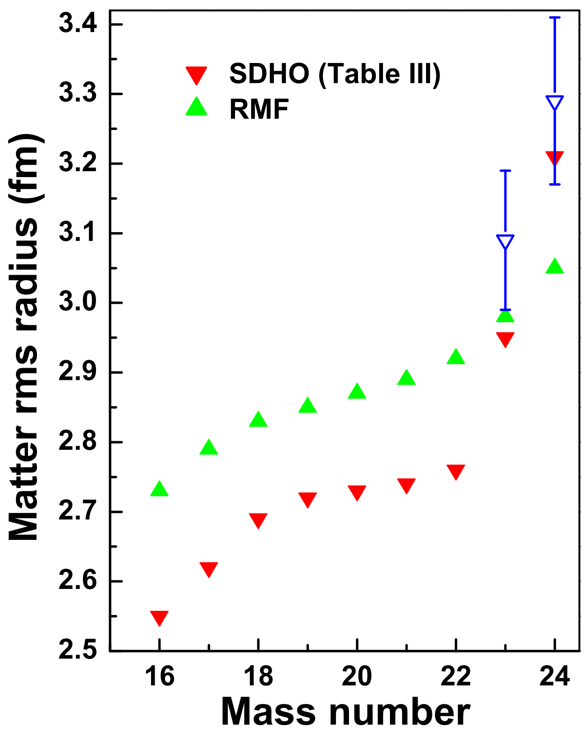

FIG. 5. Matter rms radii of $^{16-24}$O isotopes using SDHO (inverted triangles) and RMF (triangles) densities. The SDHO densities involve the values of oscillator parameters for proton and neutron distributions as given in Table III. The inverted open triangles with uncertainties are the predicted SDHO matter rms radii of ^{23,24}O that account for the interaction cross-section data on ^{23}O and ^{24}O employing the in-medium NN amplitude (see the text).

A. Effect of phase variation

To accommodate the effect of phase variation, we follow the approach of Franco and Yin [32], according to which the phase can be taken into account by multiplying the NN amplitude [Eq. (16)] by the phase factor $e^{-i\gamma_{NN}q^2/2}$ and treating the phase γ_{NN} as a free parameter. The other parameters of the NN amplitude (σ_{NN}, ρ_{NN}, and β_{NN}), corresponding to free NN scattering, are kept same as in Ref. [20]. The results of such calculations for p-^{16}O elastic scattering differential cross section at 1.0 GeV are presented in Fig. 8, and the values of phase variation parameter γ for pp and pn amplitudes are given in Table IV.

B. Effect of Pauli blocking

As already mentioned, the in-medium NN total cross section (σ_{NN}) and also the other parameters of the NN amplitude (ρ_{NN} and β_{NN}) are strongly modified by the Pauli blocking. Keeping this in mind, we use Eq. (16) for the NN amplitude and fix the in-medium value of σ_{NN} as obtained from the parametrization of Xiangzhou *et al.* [33]; the parameters ρ_{NN} and β_{NN} are varied up to the extent of getting best possible description of the p-^{16}O elastic scattering differential cross-section data at energy under consideration. These results are also shown in Fig. 8, and the corresponding parameters for pp and pn amplitudes are given in Table IV.

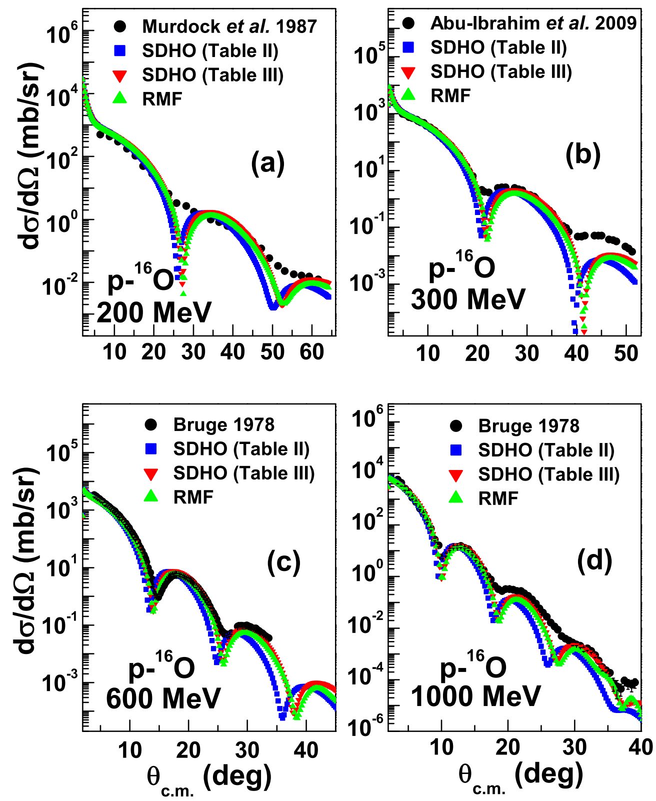

FIG. 6. Differential cross section of p-^{16}O elastic scattering at 200, 300, 600, and 1000 MeV. Squares, inverted triangles, and triangles represent the results using SDHO (Table II), SDHO (Table III), and RMF densities, respectively. The experimental data (dots) are taken from (a) Murdock *et al.* [25], (b) Abu-Ibrahim *et al.* [24], and [(c), (d)] Bruge [26].

C. Effect of higher momentum transfer components

In order to study the effects of higher momentum transfer components of NN amplitude, we consider the following

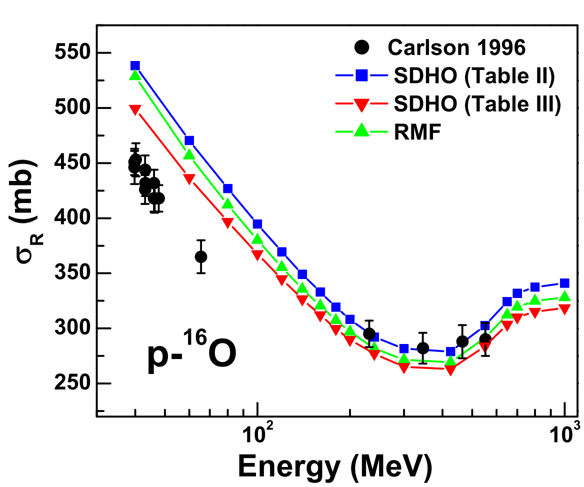

FIG. 7. Reaction cross sections of p-^{16}O scattering in the energy range 40–1000 MeV. Squares, inverted triangles, and triangles represent the results using SDHO (Table II), SDHO (Table III), and RMF densities, respectively. The experimental data (dots) are taken from Carlson [27].

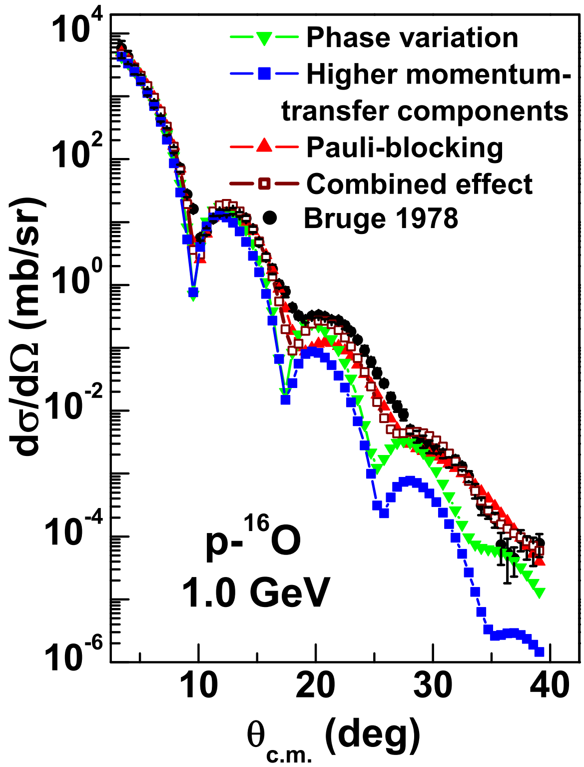

FIG. 8. Differential cross section of p-^{16}O elastic scattering at 1.0 GeV, showing the effects due to phase variation (PV) (inverted triangles), higher momentum transfer components (HMTC) (squares), and Pauli blocking (PB) (triangles) of the NN amplitude. Open squares show the combined effect of PV, HMTC, and PB. The experimental data (dots) are taken from Bruge [26].

parametrization of the NN amplitude [31]

$$f_{NN}(\vec{q}) = \frac{ik\sigma_{NN}}{4\pi}\sum_{n=0}^{\infty} A_{n+1}\left(\frac{\sigma_{NN}}{4\pi\beta_{NN}}\right)^n \times \frac{(1-i\rho_{NN})^{n+1}}{(n+1)}\exp\left[\frac{-\beta_{NN}q^2}{2(n+1)}\right], \tag{17}$$

TABLE IV. The values of NN amplitude parameters at 1.0 GeV that take care of the effects arising due to phase variation (PV), higher momentum transfer components (HMTC), and Pauli blocking (PB) of the NN amplitude.

Effect	NN	σ_{NN} (fm^2)	ρ_{NN}	β_{NN} (fm^2)	γ_{NN} (fm^2)
PV	pp	4.6300	−0.0900	0.1930	0.0954
	pn	3.8800	−0.4600	0.1510	0.4796
HMTC	pp	2.2871	−0.0451	0.1197	
	pn	3.3642	−0.3615	0.4746	
PB	pp	4.2759	−0.7843	0.1301	
	pn	3.7287	−1.1830	0.2121	
PV+HMTC+PB	pp	2.3203	−0.2373	0.1216	−0.2282
	pn	3.5650	−0.5932	0.2582	0.4367

where

$$A_{n+1} = \frac{A_1}{n(n+1)} + \frac{A_2}{(n-1)n} + \frac{A_3}{(n-2)(n-1)} + \cdots + \frac{A_n}{1.2}, \tag{18}$$

with $A_1 = 1$.

The NN amplitude [Eq. (17)] has three adjustable parameters; σ_{NN}, ρ_{NN}, and β_{NN}. These parameters along with the value of n in the summation index in Eq. (17) are varied in such a way that one is able to get the simultaneous account of the values of σ_{NN} and ρ_{NN}, corresponding to free NN scattering [20] and the p-^{16}O elastic differential cross-section data at 1.0 GeV. The results with $n = 3$ are also presented in Fig. 8, and the corresponding parameters for pp and pn amplitudes are given in Table IV.

D. Combined effect of phase variation, higher momentum transfer components, and Pauli blocking

To look into the combined effect of phase variation, higher momentum transfer components, and Pauli blocking, we parametrize the NN amplitude as follows (hereafter referred to as in-medium NN amplitude):

$$f_{NN}(\vec{q}) = \left\{\frac{ik\sigma_{NN}}{4\pi}\sum_{n=0}^{\infty} A_{n+1}\left(\frac{\sigma_{NN}}{4\pi\beta_{NN}}\right)^n \frac{(1-i\rho_{NN})^{n+1}}{(n+1)} \times \exp\left[\frac{-\beta_{NN}q^2}{2(n+1)}\right]\right\}\exp\left(\frac{-i\gamma_{NN}q^2}{2}\right). \tag{19}$$

The NN amplitude [Eq. (19)] consists of four adjustable parameters: σ_{NN}, ρ_{NN}, β_{NN}, and γ_{NN}. The variation of these parameters now allows simultaneous description of the in-medium value of σ_{NN} [33] and p-^{16}O elastic scattering differential cross-section data at energy under consideration. Such results are also depicted in Fig. 8, and the corresponding parameters of the pp and pn amplitudes are given in Table IV.

The results in Fig. 8 show that although the individual effects of phase variation, higher momentum transfer components, and Pauli blocking of the NN amplitude reflect their relative importance, the inclusion of the combined effect, however, provides quite a satisfactory explanation of p-^{16}O scattering data up to the available range of scattering angles. In order to increase the domain of our calculations and to see how far the effects of phase variation, higher momentum transfer components, and Pauli blocking of the NN amplitude are important in other situations, we consider the p-^{16}O reaction cross sections σ_R in the energy range 40–550 MeV, where the experimental data are available [27]. However, for illustration purpose, we calculate σ_R for p-^{16}O scattering only at some selective energies (40, 65, and 550 MeV). The results of such calculations are presented in Table V. It is found that the individual consideration of phase variation and Pauli blocking as well as the consideration of the combination of phase variation, higher momentum transfer components, and Pauli blocking of the NN amplitude provide equivalently good description of the experimental data at energies under consideration. Further, we notice that the consideration of higher momentum transfer components of the NN amplitude alone shows large deviations from the experimental data at

TABLE V. Effects of phase variation (PV), higher momentum transfer components (HMTC), and Pauli blocking (PB) of the NN amplitude on p-^{16}O reaction cross sections σ_R at 40, 65, and 550 MeV. $\sigma_R^{\rm th}$ and $\sigma_R^{\rm exp}$ represent our theoretical estimates and experimental values of σ_R.

Energy (MeV)	Effect	$\sigma_R^{\rm th}$ (mb)	$\sigma_R^{\rm exp}$ (mb)
40	PV	452.1	452.0 [27]
	PB	455.0	
	HMTC	533.9	
	PV+HMTC+PB	452.0	
65	PV	365.0	365.0 [27]
	PB	404.1	
	HMTC	475.4	
	PV+HMTC+PB	365.0	
550	PV	294.1	290.0 [27]
	PB	290.0	
	HMTC	348.8	
	PV+HMTC+PB	290.0	

all the considered energies. This shows that the analysis of p-^{16}O reaction cross sections may not be helpful in providing satisfactory understanding of the NN amplitude in the nuclear medium. Thus, we arrive at the conclusion that, in the present context, the study of p-^{16}O elastic differential cross section seems to be a better choice to predict the in-medium behavior of the NN amplitude.

Having obtained the in-medium parameters of the NN amplitude (Table IV), we now proceed to perform parameter free calculations for $^{16-24}$O-^{12}C interaction cross sections at 1.0 GeV/nucleon. The results of such calculations are presented in Fig. 9. It is found that, except for ^{23}O and ^{24}O, the use of SDHO densities, corresponding to RMF matter rms radii, along with the in-medium corrected NN amplitude, provides satisfactory explanation of the experimental data. Here, it should be mentioned that the results can be improved further by making some minor changes in the RMF matter rms radii of oxygen isotopes (results not shown).

Let us now focus our attention on ^{23}O and ^{24}O, whose interaction cross sections σ_I with ^{12}C are not well reproduced, even when the in-medium effects are taken into account. For if we have a look on the interaction cross sections of $^{16-24}$O, we find that the values of σ_I follow almost a systematic increase up to ^{22}O, whereas this increase becomes noticeably higher for ^{23}O and ^{24}O. Keeping this in mind, we conjecture that this feature of σ_I beyond ^{22}O might be due to relatively larger envelope of neutron distribution in the surface region of ^{23}O and ^{24}O, as compared to the ones obtained using SDHO densities corresponding to RMF neutron rms radii. In other words, we expect that both ^{23}O and ^{24}O may require larger matter rms radii, as compared to their RMF values, to accommodate the increasing trend of σ_I beyond ^{22}O. To incorporate this in the calculations and to see how far it helps in the present context, we consider the increase in SDHO matter rms radii of ^{23}O and ^{24}O by varying the oscillator parameter for neutron distribution. The results of such calculations show that the matter rms radii of ^{23}O and ^{24}O that can account for the interaction cross section data are 3.08 ± 0.10 fm and 3.28 ± 0.12 fm, respectively (shown in Fig. 5); the coresponding values of the neutron skin thickness in ^{23}O and ^{24}O are found to be 0.68 ± 0.14 fm and 0.93 ± 0.17 fm, respectively. We find that the predicted SDHO matter rms radii of ^{23}O and ^{24}O are reasonably larger than the RMF values (Table I). Further, the results predict thicker neutron skins in ^{23}O and ^{24}O as compared to RMF ones. The detailed analysis presented herein thus establishes the utility of SDHO densities in predicting the matter rms radii of neutron-rich nuclei.

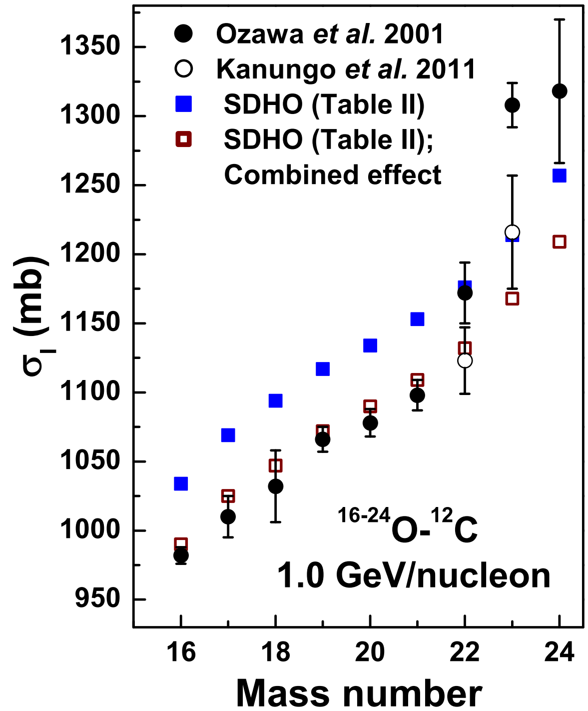

FIG. 9. Interaction cross sections of $^{16-24}$O isotopes on a ^{12}C target at 1.0 GeV/nucleon. Squares show the results using SDHO densities (involving the values of oscillator parameters for proton and neutron distributions as given in Table II) and the free NN amplitude. Open squares show the results using similar SDHO densities as used in obtaining squares, but involve the combined effect of the phase variation, higher momentum transfer components, and Pauli blocking of the NN amplitude. The experimental data (dots and open circles) are taken from Ozawa *et al.* [2] and Kanungo *et al.* [10].

IV. SUMMARY AND CONCLUSIONS

In this work, we have presented a theoretical study of the interaction cross sections of oxygen isotopes from ^{12}C target at 1.0 GeV/nucleon, using the Coulomb modified correlation expansion for the Glauber model S matrix for nucleus-nucleus scattering. The densities of the colliding nuclei are obtained using (i) the Slater determinants consisting of the harmonic oscillator single-particle wave functions (SDHO) and (ii) the relativistic mean field (RMF) approach. By retaining up to the two-body density term in the correlation expansion, the calculations are performed using the free as well as the in-medium nucleon-nucleon (NN) scattering amplitude. The in-medium NN amplitude considers the effects arising due to phase variation, higher momentum transfer components, and Pauli blocking. Our main concern in this work is to see how could one make the best use of SDHO densities with reference to RMF one and how far the simple (single parameter) SDHO densities account for the experimental data. The results show that the use of SDHO densities, along with the in-medium corrected NN amplitude, provides satisfactory explanation of the experimental data. It is found that, except for ^{23,24}O, the predicted SDHO matter rms radii of oxygen isotopes closely agree with those obtained using the RMF densities. However, for ^{23}O and ^{24}O, our results require reasonably larger SDHO matter rms radii than the RMF values. This result predicts thicker neutron skins in ^{23}O and ^{24}O as compared to RMF ones.

Thus, we conclude that the present analysis establishes the utility of SDHO densities in providing fairly reliable estimates of the matter rms radii of neutron-rich nuclei. Using a similar approach, we aim to predict the matter rms radii of all such neutron-rich nuclei in near future.

ACKNOWLEDGMENTS

S.A. gratefully acknowledges financial support in the form of a research fellowship from the University Grants Commission (UGC), Government of India. A.A.U. acknowledges the Inter-University Centre for Astronomy and Astrophysics, Pune, India, for support via an associateship and for hospitality. We thank Tabassum Naz for providing RMF densities for oxygen isotopes in tabular form.

APPENDIX: INTRINSIC MATTER DENSITY DISTRIBUTIONS

1. Proton density distributions

$$\rho_{^{16-26}O}(r) = \frac{1}{\pi^{3/2}p^3}\left[1 - \frac{3}{16\alpha^2 p^2} + \frac{1}{32}\frac{r^2}{\alpha^2 p^4}\right]\exp\left(-\frac{r^2}{4p^2}\right). \tag{A1}$$

2. Neutron density distributions

$$\rho_{^{17}O}(r) = \frac{1}{8\pi^{3/2}p^3}\left[9 - \frac{2}{\alpha^2 p^2} + \frac{1}{16\alpha^4 p^4} + \left(\frac{1}{3\alpha^2 p^4} - \frac{1}{48\alpha^4 p^6}\right)r^2 + \frac{1}{960}\frac{r^4}{\alpha^4 p^8}\right]\exp\left(-\frac{r^2}{4p^2}\right), \tag{A2}$$

$$\rho_{^{18}O}(r) = \frac{1}{8\pi^{3/2}p^3}\left[10 - \frac{5}{2\alpha^2 p^2} + \frac{1}{8\alpha^4 p^4} + \left(\frac{5}{12\alpha^2 p^4} - \frac{1}{24\alpha^4 p^6}\right)r^2 + \frac{1}{480}\frac{r^4}{\alpha^4 p^8}\right]\exp\left(-\frac{r^2}{4p^2}\right), \tag{A3}$$

$$\rho_{^{19}O}(r) = \frac{1}{8\pi^{3/2}p^3}\left[11 - \frac{3}{\alpha^2 p^2} + \frac{3}{16\alpha^4 p^4} + \left(\frac{1}{2\alpha^2 p^4} - \frac{1}{16\alpha^4 p^6}\right)r^2 + \frac{1}{320}\frac{r^4}{\alpha^4 p^8}\right]\exp\left(-\frac{r^2}{4p^2}\right), \tag{A4}$$

$$\rho_{^{20}O}(r) = \frac{1}{8\pi^{3/2}p^3}\left[12 - \frac{7}{2\alpha^2 p^2} + \frac{1}{4\alpha^4 p^4} + \left(\frac{7}{12\alpha^2 p^4} - \frac{1}{12\alpha^4 p^6}\right)r^2 + \frac{1}{240}\frac{r^4}{\alpha^4 p^8}\right]\exp\left(-\frac{r^2}{4p^2}\right), \tag{A5}$$

$$\rho_{^{21}O}(r) = \frac{1}{8\pi^{3/2}p^3}\left[13 - \frac{4}{\alpha^2 p^2} + \frac{5}{16\alpha^4 p^4} + \left(\frac{2}{3\alpha^2 p^4} - \frac{5}{48\alpha^4 p^6}\right)r^2 + \frac{1}{192}\frac{r^4}{\alpha^4 p^8}\right]\exp\left(-\frac{r^2}{4p^2}\right), \tag{A6}$$

$$\rho_{^{22}O}(r) = \frac{1}{8\pi^{3/2}p^3}\left[14 - \frac{9}{2\alpha^2 p^2} + \frac{3}{8\alpha^4 p^4} + \left(\frac{3}{4\alpha^2 p^4} - \frac{1}{8\alpha^4 p^6}\right)r^2 + \frac{1}{160}\frac{r^4}{\alpha^4 p^8}\right]\exp\left(-\frac{r^2}{4p^2}\right), \tag{A7}$$

$$\rho_{^{23}O}(r) = \frac{1}{8\pi^{3/2}p^3}\left[15 - \frac{5}{\alpha^2 p^2} + \frac{17}{32\alpha^4 p^4} + \left(\frac{5}{6\alpha^2 p^4} - \frac{17}{96\alpha^4 p^6}\right)r^2 + \frac{17}{1920}\frac{r^4}{\alpha^4 p^8}\right]\exp\left(-\frac{r^2}{4p^2}\right), \tag{A8}$$

$$\rho_{^{24}O}(r) = \frac{1}{8\pi^{3/2}p^3}\left[16 - \frac{11}{2\alpha^2 p^2} + \frac{11}{16\alpha^4 p^4} + \left(\frac{11}{12\alpha^2 p^4} - \frac{11}{48\alpha^4 p^6}\right)r^2 + \frac{11}{960}\frac{r^4}{\alpha^4 p^8}\right]\exp\left(-\frac{r^2}{4p^2}\right), \tag{A9}$$

$$\rho_{^{25}O}(r) = \frac{1}{8\pi^{3/2}p^3}\left[17 - \frac{6}{\alpha^2 p^2} + \frac{3}{4\alpha^4 p^4} + \left(\frac{1}{\alpha^2 p^4} - \frac{1}{4\alpha^4 p^6}\right)r^2 + \frac{1}{80}\frac{r^4}{\alpha^4 p^8}\right]\exp\left(-\frac{r^2}{4p^2}\right), \tag{A10}$$

$$\rho_{^{26}O}(r) = \frac{1}{8\pi^{3/2}p^3}\left[18 - \frac{13}{2\alpha^2 p^2} + \frac{13}{16\alpha^4 p^4} + \left(\frac{13}{12\alpha^2 p^4} - \frac{13}{48\alpha^4 p^6}\right)r^2 + \frac{13}{960}\frac{r^4}{\alpha^4 p^8}\right]\exp\left(-\frac{r^2}{4p^2}\right), \tag{A11}$$

Here,

$$p^2 = \frac{A-1}{4\alpha^2 A}. \tag{A12}$$

The quantities α^2 and A in the above equations are the oscillator parameter and number of nucleons in the nucleus, respectively.

[1] I. Tanihata, H. Hamagaki, O. Hashimoto, Y. Shida, N. Yoshikawa, K. Sugimoto, O. Yamakawa, T. Kobayashi, and N. Takahashi, Phys. Rev. Lett. **55**, 2676 (1985).
[2] A. Ozawa, T. Suzuki, and I. Tanihata, Nucl. Phys. A **693**, 32 (2001).
[3] I. Tanihata *et al.*, Phys. Lett. B **206**, 592 (1988).
[4] M. Fukuda *et al.*, Phys. Lett. B **268**, 339 (1991).
[5] T. Nakamura, N. Fukuda, T. Kobayashi, N. Aoi, H. Iwasaki, T. Kubo, A. Mengoni, M. Notani, H. Otsu, H. Sakurai, S. Shimoura, T. Teranishi, Y. X. Watanabe, K. Yoneda, and M. Ishihara, Phys. Rev. Lett. **83**, 1112 (1999).
[6] A. H. Wapstra, G. Audi, and C. Thibault, Nucl. Phys. A **729**, 129 (2003).
[7] K. Tanaka *et al.*, Phys. Rev. Lett. B **104**, 062701 (2010).
[8] M. Sharma, A. Bhagwat, Z. A. Khan, W. Haider, and Y. K. Gambhir, Phys. Rev. C **83**, 031601(R) (2011).
[9] D. Chauhan, Z. A. Khan, and A. A. Usmani, Phys. Rev. C **90**, 024603 (2014).
[10] R. Kanungo, A. Prochazka, M. Uchida, W. Horiuchi, G. Hagen, T. Papenbrock, C. Nociforo, T. Aumann, D. Boutin, D. Cortina-Gil, *et al.*, Phys. Rev. C **84**, 061304(R) (2011).
[11] S. Ahmad, D. Chauhan, A. A. Usmani, and Z. A. Khan, Eur. Phys. J. A **52**, 128 (2016).
[12] W. Czyz and L. C. Maximon, Ann. Phys. (NY) **52**, 59 (1969).
[13] V. Franco and G. K. Varma, Phys. Rev. C **18**, 349 (1978).
[14] I. Ahmad, J. Phys. G **6**, 947 (1980).
[15] V. Franco and G. K. Varma, Phys. Rev. C **12**, 225 (1975).
[16] G. Fäldt and H. Pilkuhn, Phys. Lett. B **46**, 337 (1973).
[17] A. Ozawa *et al.*, Nucl. Phys. A **709**, 60 (2002).
[18] Z. A. Khan and Minita Singh, Int. J. Mod. Phys. E **16**, 1741 (2007).
[19] G. D. Alkhazov *et al.*, Nucl. Phys. A **712**, 269 (2002).
[20] B. Abu-Ibrahim, W. Horiuchi, A. Kohama, and Y. Suzuki, Phys. Rev. C **77**, 034607 (2008).
[21] W. Horiuchi, Y. Suzuki, B. Abu Ibrahim, and A. Kohama, Phys. Rev. C **75**, 044607 (2007); **76**, 039903(E) (2007).
[22] G. A. Lalazissis *et al.*, Phys. Lett. B **671**, 36 (2009).
[23] A. Karim and S. Ahmad, Phys. Rev. C **92**, 064608 (2015).
[24] B. Abu-Ibrahim *et al.*, J. Phys. Soc. Jpn. **78**, 044201 (2009).
[25] D. P. Murdock and C. J. Horowitz, Phys. Rev. C **35**, 1442 (1987).
[26] G. Bruge, Int. Report DPh-N/ME 1978-1 CEN, Saclay, BP 2, 91190 Gif-sur-Yvette, France, 1978 (unpublished).
[27] R. F. Carlson, At. Data Nucl. Data Tables **63**, 93 (1996).
[28] I. Sick and J. S. McCarthy, Nucl. Phys. A **150**, 631 (1970).
[29] G. Q. Li and R. Machleidt, Phys. Rev. C **48**, 1702 (1993); **49**, 566 (1994).
[30] C. A. Bertulani, J. Phys. G **27**, L67 (2001).
[31] D. Chauhan and Z. A. Khan, Phys. Rev. C **75**, 054614 (2007).
[32] V. Franco and Y. Yin, Phys. Rev. Lett. **55**, 1059 (1985).
[33] C. Xiangzhou, F. Jun, S. Wenqing, M. Yugang, W. Jiansong, and Y. Wei, Phys. Rev. C **58**, 572 (1998).